

Interfacial Microstructure and Mechanical Properties of Friction Stir Welded Joints of Commercially Pure Aluminum and 304 Stainless Steel

Balamagendiravarman Murugan, Gopinath Thirunavukarasu, Sukumar Kundu, Satish V. Kailas, and Subrata Chatterjee

(Submitted August 26, 2016; in revised form April 16, 2018; published online May 2, 2018)

In the present investigation, friction stir welding of commercially pure aluminum and 304 stainless steel was carried out at varying tool rotational speeds from 200 to 1000 rpm in steps of 200 rpm using 60 mm/min traverse speed at 2 (degree) tool tilt angle. Microstructural characterization of the interfacial zone was carried out using optical microscope and scanning electron microscope. Energy-dispersive spectroscopy indicated the presence of FeAl₃ intermetallic phase. Thickness of the intermetallic layer increased with the increase in tool rotational speed. X-ray diffraction studies indicated the formation of intermetallic phases like FeAl₂, Fe₄Al₁₃, Fe₂Al₅, and FeAl₃. A maximum tensile strength of ~ 90% that of aluminum along with ~ 4.5% elongation was achieved with the welded sample at tool rotational speed of 400 rpm. The stir zone showed higher hardness as compared to base metals, heat affected zone, and thermo-mechanically affected zone due to the presence of intermetallics. The maximum hardness value at the stir zone was achieved at 1000 rpm tool rotational speed.

Keywords dissimilar metals, friction stir welding, mechanical properties, microstructure, weld nugget

1. Introduction

Friction stir welding (FSW) is a solid-state joining process and is considered to be the most significant progress in metal joining in the past few decades due to its energy efficiency, environmental friendliness, and versatility (Ref 1). FSW is of significant importance especially for joining of dissimilar metals with wide difference in thermal and mechanical properties. However, joining of dissimilar metals involves severe flaws like the formation of brittle intermetallic compounds (Ref 2-4). Joining of dissimilar metals is more challenging than that of similar metals due to variation in properties, but is often required to meet the growing industrial needs (Ref 5). FSW came in the limelight for joining of low and high melting point metals as it helps to solve the complex functional problems in joining of dissimilar materials. Aluminum has good heat transfer property, good formability and low weight that are vital for aerospace industries, automobile parts, and some naval components. Stainless steel possesses high strength, high corrosion resistance, and high toughness. Stainless steel is a significant structural material extensively used in automotive and aerospace industry. FSW of stainless steel and aluminum is attractive, because such joints provide the design engineers an opportunity to explore their applica-

tions in the field of cryogenics where cryogenic liquid is stored in Al chambers and transferred through SS pipeline (Ref 6-8). Nuclear industry is also looking forward to SS-Al assembly to fabricate neutron sensitive ion chambers (Ref 9). Combinations of aluminum and stainless steel are potential candidates for developing industrial products especially in automobile industry due to their high strength-to-weight ratio leading to higher fuel efficiency (Ref 10-12). FSW of Al 6061-T6 and SS (STS304) at tool rotational speeds of 300-600 rpm and travel speed of 48 mm/min were reported (Ref 13). Ghosh et al. (Ref 3) used varying tool rotational speeds from 560 to 900 rpm for joining of 6061 Al and 304 stainless steel. Chen (Ref 14) used traverse speeds of 54, 72, and 90 mm/min in joining of aluminum to steel and the minimum traverse speed gave the best impact values and acceptable values of tensile strength. Tool rotational speed and tool feed rate are significant parameters in making a sound joint. Habibnia et al. (Ref 2) employed variations in offset as 0, 0.8, and 1.5 mm for joining of 304 SS and 5050Al. The offset was provided with an aim to reduce overheating and pin erosion. They reported that at zero offset cracks were formed, at 0.8 mm offset tunnel defects were observed and for 1.5 mm tool offset, rotational movement of tool abraded the edge of steel sheet that effected a uniform distribution of steel particles in the stir zone due to small size of the steel particles and consequently lesser defects resulted in the stir zone (Ref 2). The possible intermetallic phases formed at the interface were reported to be FeAl, Fe₂Al₅, FeAl₂, FeAl₃, and Fe₄Al₁₃ (Ref 15-17). However, brittle Al-rich intermetallic compounds were formed at the interface of aluminum and steel joints due to intermixing of materials during welding and it was reported that the thicker intermetallic layers lead to failure of the joint under stressed conditions (Ref 18). Ghosh et al. (Ref 9) have performed the joining of CP Al-304SS at 1000 rpm for traverse speed of 50 mm/min. However, report on the effect of tool rotational speed on joining of dissimilar material CP Al and 304SS is scanty in the literature. In the present study, FSW of commercial pure aluminum and 304SS with tool rotational

Balamagendiravarman Murugan, Gopinath Thirunavukarasu, Sukumar Kundu, and Subrata Chatterjee, Department of Metallurgy and Materials Engineering, Indian Institute of Engineering Science and Technology, Shibpur, Howrah 711103, India; **Satish V. Kailas**, Department of Mechanical Engineering, Indian Institute of Science, Bengaluru 560012, India. Contact e-mails: skundu@metal.iests.ac.in and erskundu@gmail.com.

speeds from 200 to 1000 rpm in steps of 200 rpm at 60 mm/min traverse speed was carried out. In this study, microstructure of different zones, formation of intermetallic phases, microhardness, tensile strength, and fracture morphologies of the FSW joints has been investigated.

2. Experimental Procedure

Commercially pure aluminum (CP Al) and 304 stainless steel (304SS) sheets having dimensions of 160 mm length \times 60 mm width \times 3 mm thickness were used in this investigation. The chemical composition of CP Al is Al-0.02Fe-0.2Si-0.003Mn-0.002S-0.002P-0.005N (wt.%) and of 304SS is Fe-18.2Cr-8.4Ni-1.34Mn-0.04C-0.4Si (wt.%). The sheets were cleaned with ethanol and then mounted on the machine to make a butt joint. CP Al was placed on the retreating side and 304SS on advancing side. The welding direction was parallel to the rolling direction of the sheets. A tungsten carbide tool with a shoulder diameter of 25 mm, conical probe of 6 mm diameter, and pin length of 2.7 mm was used for the welding process. The welding tool was tilted 2° angle forward from the vertical and shifted toward the Al side with an offset of \sim 1.25 mm as shown in Fig. 1. The two major reasons for providing the offset were to avoid tool breakage while plunging at the interface due to higher strength of stainless steel side with respect to aluminum side and also to avoid superheating of aluminum due to the difference in the material flow behavior of the two materials. FSW was performed at tool rotational speeds of 200-1000 rpm in steps of 200 rpm, with a travel speed of 60 mm/min. Both base metals and welded samples were prepared by conventional metallographic techniques. CP Al side was first etched using Keller's reagent, and then 304SS side was etched using aqua regia. Microstructures of the welded samples were examined with an optical microscope. The polished interface of the welded joint was examined using a scanning electron microscope SEM (JEOL JSM-5510) in backscattered mode. Energy-dispersive spectroscopy (NORAN System Six) was used to determine the chemical composition of the interface. X-ray diffraction (Philips PW 1830) technique was used to conform the phases predicted. To evaluate the mechanical properties, tensile and micro-hardness tests were carried out. Tensile test of the welded joints was carried out in an Instron 4204 machine at a constant crosshead speed of 1.67×10^{-3} mm/s. The tensile samples were prepared according to the ASTM E8M-11 standard. Microhardness was measured along the transverse section of the welded specimen using a diamond micro-indenter with a load of 100 gf and dwell time of 20 s. Indentations were made at mid-section of the welded joints. The fracture surfaces of the welded samples

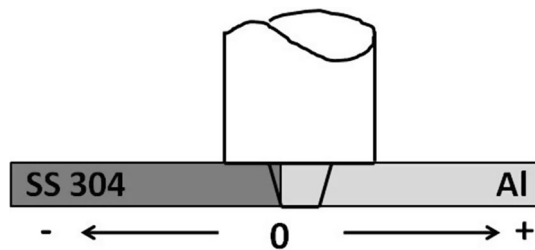


Fig. 1 Schematic illustration of tool offset position for FSW

were examined by SEM (Hitachi S 3400) in secondary electron mode.

3. Results and Discussion

3.1 Microstructural Characterization

The surfaces of the friction stir welded samples processed at varying rotational speeds are shown in Fig. 2. The welded surface at lower rotational speed experienced less amount of heat generation during stirring action (Fig. 2a and b). However, at higher rotational speeds flashes were formed due to greater heat generation as shown in Fig. 2(c), (d), and (e).

The optical photomicrographs of friction stir welded joints are shown in Fig. 3. Three zones are formed during welding: heat affected zone (HAZ), thermo-mechanically affected zone (TMAZ), and stir zone (SZ). The microstructure of HAZ region at the stainless steel side does not show much difference as compared to base material. The grains are elongated in the TMAZ due to deformation. At the stir zone, the grains are finer due to the stirring action of the pin. At the retreating side, more reaction takes place due to shifting of pin toward the CP Al side. So, more plastic deformation occurs on the CP Al side. Stainless steel particles of different size were distributed over the CP Al side due to stirring action of the pin. These particles are irregular in shape and unevenly distributed. Cracks are formed on the steel particles as a result of high deformation and mixing of materials (Ref 6). The grains formed in the stir zone of aluminum side are fine, equiaxial, and of recrystallized structure. At higher rotational speeds, the grains are coarser due to severe plastic deformation followed by recrystallization on

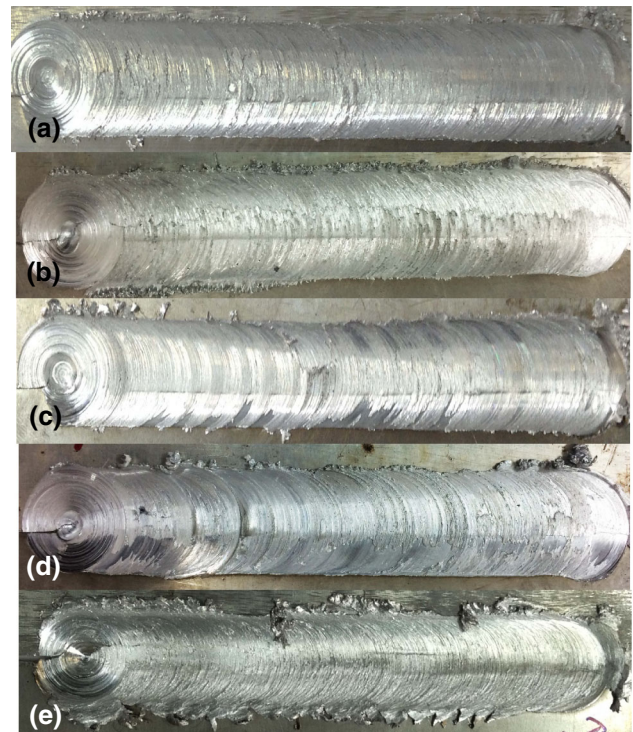


Fig. 2 Surface view of the welded joints at varying tool rotational speeds (a) 200 rpm, (b) 400 rpm, (c) 600 rpm, (d) 800 rpm and (e) 1000 rpm

the aluminum side (Ref 19, 20). The average grain sizes of the different welded zones for varying tool rotational speeds are shown in Fig. 4. Hassan et al. (Ref 21) reported that the grain structure is very finer at lower heat inputs, whereas at higher heat inputs the grain structure is coarser due to grain growth. Hence, the grain size at lower rotational speeds is finer as compared to that of higher tool rotational speeds.

The SEM images of the friction stir welded joints are shown in Fig. 5. Intermetallic compounds are formed at the stir zone due to the thermal and mechanical action that took place in the material during stirring of the pin. The images were taken at the interfacial region of the welded sample. Figure 5(a) shows intermetallic layer thickness (marked by arrow) at lower rotational speed which is much less compared to that at higher rotational speed (Fig. 5f). This demonstrates that the intermetal-

lic layer thickness increases with increase in rotational speed (Ref 22). Figure 5(b) exhibits an insignificant amount of aluminum particles at 304SS side besides the interface, but steel particles were observed at the CP Al side (Fig. 5c). This is due to the fact that 304SS was placed at the advancing side and CP Al at the retreating side, the tool rubbed the surface of the 304SS and pulled the steel particles over to the CP Al side. The other reason could be the 1.25 mm offset of the tool toward the CP Al side; hence, there was no significant structural change in the stainless steel side. In Fig. 5(d) and (e), steel particles are observed in broken condition that can be attributed to rotation of the pin and the plastically deformed aluminum trying to fill the gaps.

The peak temperature at the interface was described by Arbegast et al. (Ref 23) and expressed by the equation

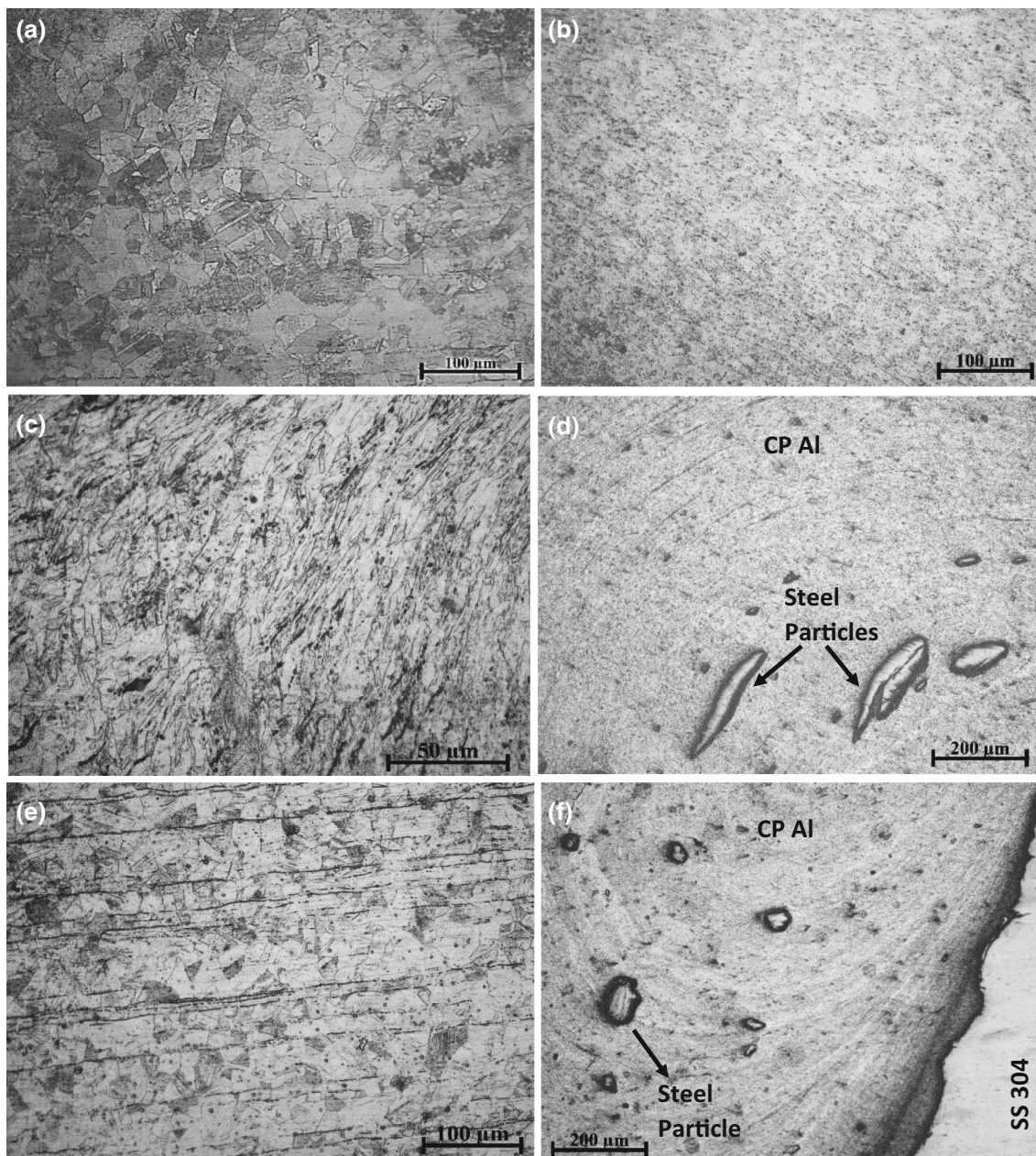


Fig. 3 Optical photomicrograph of varying tool rotational speeds at (a) HAZ of SS side at 400 rpm, (b) TMAZ of aluminum side at 400 rpm, (c) TMAZ of SS side at 600 rpm, (d) SZ of aluminum side at 800 rpm, (e) SZ of SS side at 600 rpm and (f) interface region at 1000 rpm

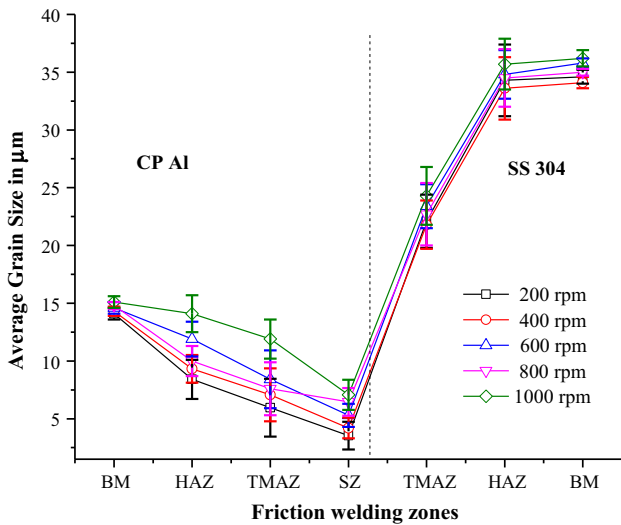


Fig. 4 The average grain size of different welding zones for varying rotational speed at 60 mm/min traverse speed

$$\frac{T}{T_m} = K \left[\frac{\omega^2}{V \cdot 10^4} \right]^\alpha$$

where T is the temperature during welding, T_m is the melting point of the alloy, V is the traversing speed of the tool (mm/s), α is a constant and considered as 0.04, and K is a constant considered as 0.65 (Ref 3, 23). The temperatures at the interface for varying tool rotational speeds are given in Table 1. The temperatures at the interface indicate the prospect of formation of intermetallic phases like FeAl_3 , Fe_2Al_5 , FeAl_2 , and $\text{Fe}_4\text{Al}_{13}$ that is vindicated from Al-Fe phase diagram (Ref 24).

The quantitative analysis of friction stir welded samples is shown in Fig. 6. Figure 6(a) shows that the steel particles were distributed in the aluminum side and the particles comprised of Al (71–78 wt.%), Fe (18–21 wt.%) (at point 1), Al (~ 97 wt.%) Fe (~ 3 wt.%) (at point 2), Al (~ 16 wt.%), Fe (~ 72 wt.%), Cr (~ 8 wt.%), Ni (~ 4 wt.%) (at point 3) and Al (~ 42 wt.%), Fe (~ 51 wt.%), Cr (~ 5 wt.%), Ni (~ 2 wt.%) (at point 4), so the phases observed are FeAl_3 , Al, FeAl, and FeAl, respectively. Figure 6(b) shows that the cracks were formed within the steel particles and intrusion of aluminum particle had taken place. The composition of the particles is Al (~ 19 wt.%), Fe (~ 58 wt.%), Cr (~ 7 wt.%), Ni (~ 4 wt.%) (at point 1), Al (~ 93 wt.%), Fe (~ 7 wt.%) (at point 2), Al (~ 98 wt.%), Fe (~ 2 wt.%) (at point 3), Al (~ 38 wt.%), Fe (~ 53 wt.%), Cr (~ 6 wt.%), Ni (~ 3 wt.%) (at point 4), Al (~ 12 wt.%), Fe (~ 78 wt.%), Cr (~ 6 wt.%), Ni (~ 4 wt.%) (at point 5), and Al (~ 13 wt.%), Fe (~ 65 wt.%), Cr (~ 8 wt.%) and Ni (~ 4 wt.%) (at point 6), so the formation of FeAl_3 , Al, Al, FeAl, Fe, and FeAl_3 phases, respectively, are confirmed (Ref 9). The compositions of the intermetallic phases were determined from Al-Fe, Al-Cr binary phase diagrams (Ref 24). The phases have major quantity of Al with considerable quantity of Fe and very less of Cr and Ni which indicates insignificant influence of chromium and nickel in the formation of phases. The line profile of the interface region is shown in Fig. 6(c) and summarized in Fig. 7. On 304SS side, the material flow was within the interface region and the interface took a non-linear shape. The formation of

non-linear shape, according to Lee et al. (Ref 25), is due to stirring of the steel side by the outer edge of the pin. Figure 7 shows an increase in aluminum content (in counts) at the cracks of the SS side due to the extrusion of the pin and the plastically deformed aluminum trying to fill the gaps. The intermetallic phase formed at the interfacial zone (vide Fig. 6d) consists of Al (~ 66 wt.%), Fe (~ 24 wt.%), Ni (~ 2.4 wt.%), and Cr (~ 3.5 wt.%). This composition indicates the formation of FeAl_3 intermetallic phase, which is Al-rich phase (Ref 22, 26). Yazdipour et al. (Ref 27) reported the formation of FeAl_3 intermetallic compound at the interface while joining aluminum 5083-H321 and 316L.

Figure 8 shows x-ray diffraction patterns of the friction stir welded joints at varying rotational speeds. The phases like FeAl_2 , $\text{Fe}_4\text{Al}_{13}$, and Fe_2Al_5 were observed in the welded joints. While FeAl_3 intermetallic phase was observed in SEM micrographs, $\text{Fe}_4\text{Al}_{13}$ and Fe_2Al_5 intermetallics were not observed presumably due to low volume fraction. Sahim (Ref 28) reported the formation of FeAl_3 phase in FSW of aluminum and AISI 304. Ghosh et al. (Ref 3) have reported that the formation of phases: FeAl_2 , Fe_2Al_5 , and Fe_3Al between Al 6061 and SS304 in friction stir welded joints. However, Elrefaey et al. (Ref 16) reported the formation of intermetallic phases like $\text{Fe}_4\text{Al}_{13}$ and Fe_2Al_5 in friction stirred lap joint of aluminum and steel. The structure and morphology of intermetallic phases were investigated by Bozzi et al. (Ref 29) for joining of Al and 6016/IF-steel, and the precipitates were confirmed to be either FeAl_2 (rhombohedral phase), Fe_2Al_5 (orthorhombic phase) or FeAl_3 (monoclinic phase). Agudo et al. (Ref 30) observed that most of the FeAl_3 precipitates contained a large amount of microtwins arising probably due to high stress generated by the volume expansion associated with the formation of the FeAl_3 phase.

3.2 Mechanical Properties

Tensile tests were performed at room temperature for the base metals and the joint samples. The results are shown in Fig. 9. Maximum tensile strength of ~ 119.7 MPa was obtained at 400 rpm tool rotational speed, which was about 90% of the CP Al. Ghosh et al. (Ref 9) have reported an ultimate tensile strength (UTS) value of 82% of the parent Al (UTS-74 MPa) for CP Al-304SS FSW joint. Yilmaz et al. (Ref 31) have obtained ~ 88 MPa bond strength in friction welding of CP aluminum to 304SS. Yazdipour et al. (Ref 27) have reported tensile strength of ~ 75% of the base material while joining of aluminum 5083-H321 and 316L. However, with increase in the rotational speed, the tensile strength decreased gradually and the minimum tensile strength of ~ 78 MPa was achieved at 1000 rpm tool rotational speed.

Figure 10 shows the summary of tensile strength results with varying tool rotational speeds from 200 to 1000 rpm. The maximum tensile strength was achieved at a tool rotational speed of 400 rpm. At higher tool rotational speeds, more deformation and high mixing of materials occur that leads to the formation of brittle intermetallic compounds. To eliminate excess melting phenomena in the weld nugget and in order to get good tensile strength, the tool rotational speed should be low. The intermetallic layer thickness for tool rotational speed of 1000 rpm was ~ 4.80 μm , whereas ~ 0.7 μm for 400 rpm. At 200 rpm, intermetallic layer was not observed due to low heat input and mixing of materials. Yilmaz et al. (Ref 31) reported that the tensile stress is highly influenced by the

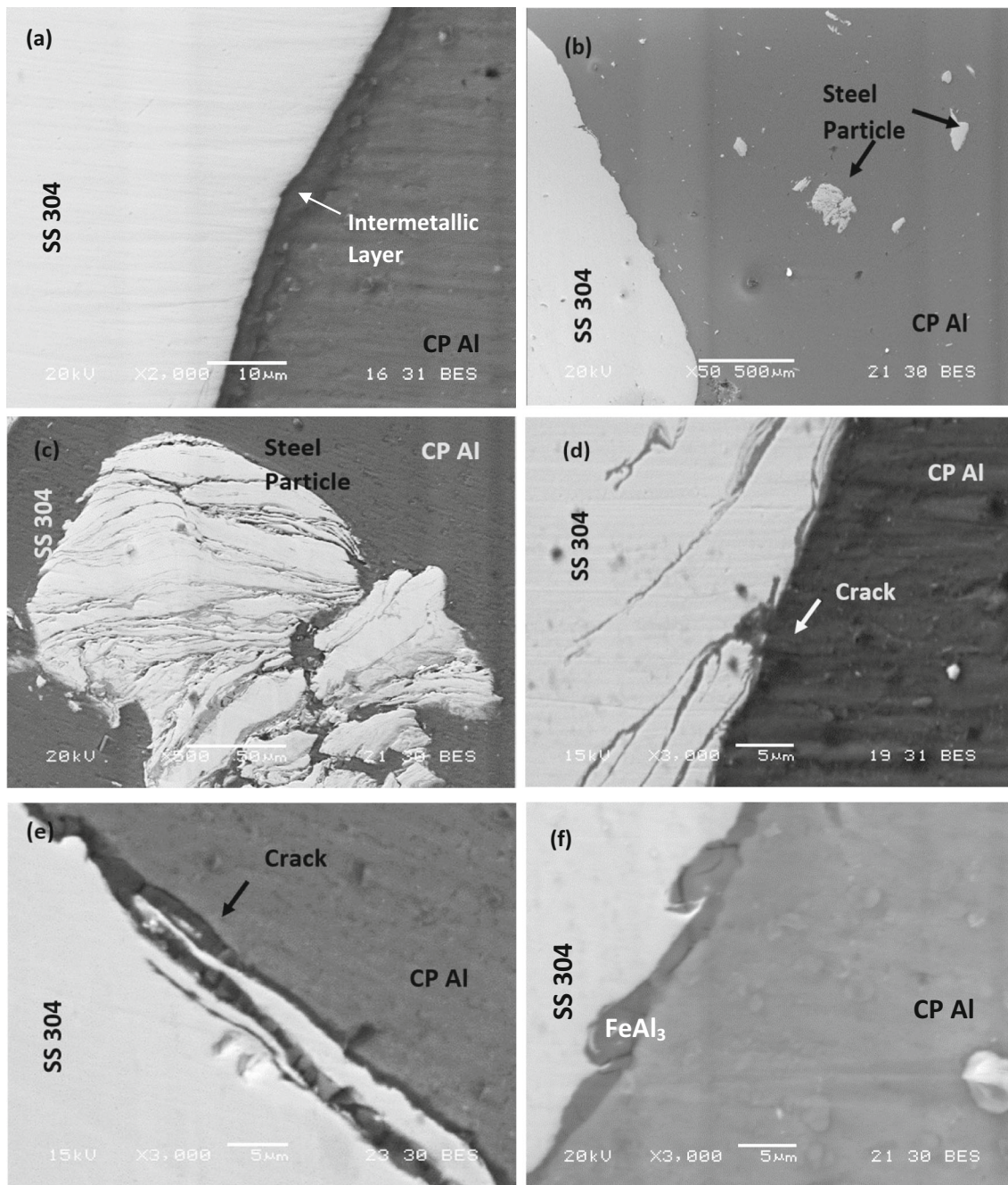


Fig. 5 SEM–BSE images of varying tool rotational speeds (a) interface region of welded joint at 200 rpm, (b) interface region of welded joint at 400 rpm, (c) SS particle on the aluminum side at 400 rpm, (d) interface region of welded joint at 600 rpm, (e) interface region of welded joint at 800 rpm and (f) reaction region at 1000 rpm

Table 1 Temperature at the interface during friction stir welding

Tool rotational speed, rpm	Maximum temperature at interface, K
200	641
400	677
600	700
800	716
1000	729

intermetallic layer thickness at the reaction zone of the welded joint and increase in layer thickness leads to a decrease in tensile strength.

The fracture surface of friction stir welded joints of CP Al side and 304SS side are shown in Fig. 11 and 12, respectively. The fractograph shows dimples at the center of the joint which indicates ductile fracture. The flat flakes observed at the bottom of the joint indicate brittle fracture.

Microhardness was measured across the cross section at the center of the friction stir welded joints, and successive

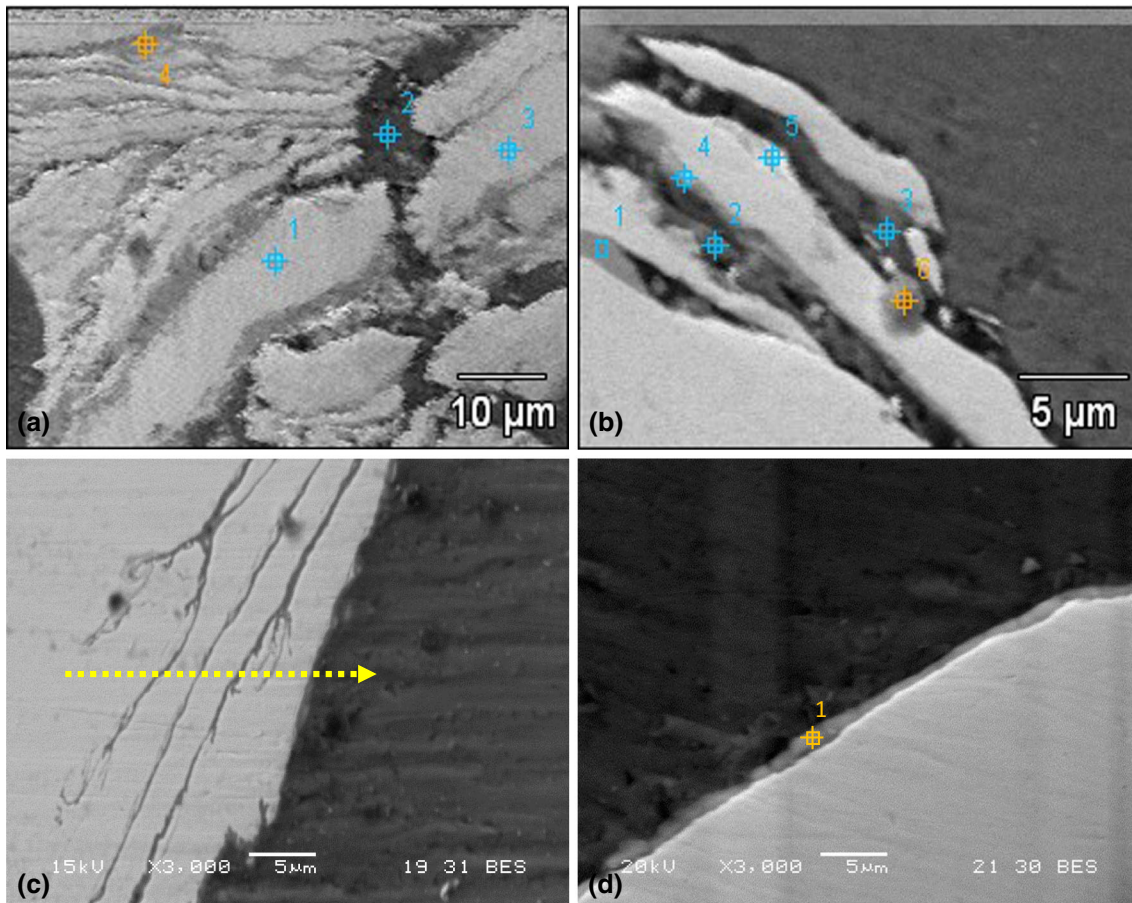


Fig. 6 Energy-dispersive spectroscopy images (a) SS particle on aluminum side at 400 rpm, (b) interface region at 600 rpm, (c) line scan of interface region at 800 rpm, and (d) interface region at 1000 rpm

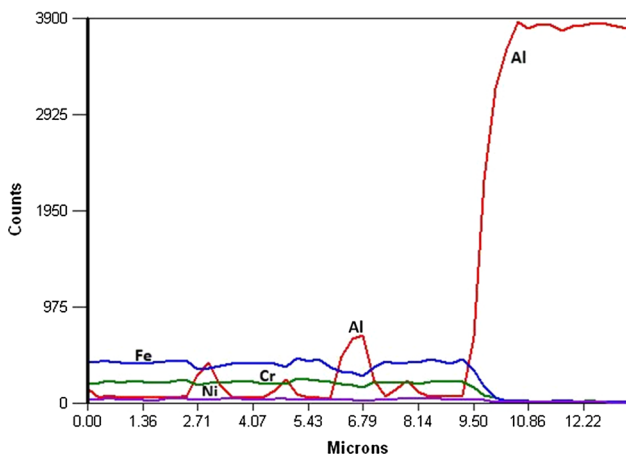


Fig. 7 SEM-EDS line scan showing composition gradients across the interface; taken along the line at 800 rpm

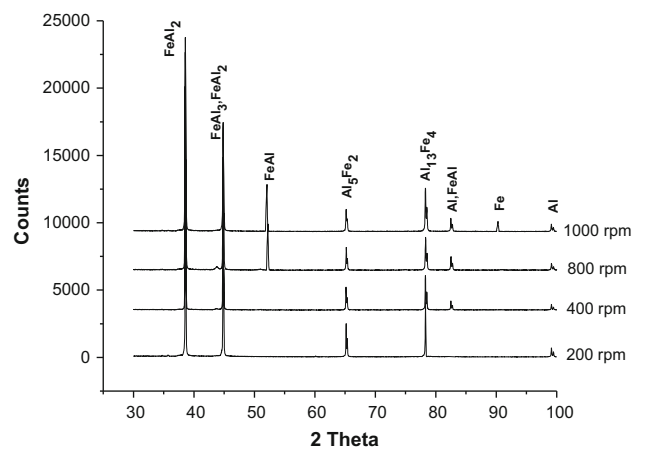


Fig. 8 XRD pattern of welded sample for varying tool rotational speeds at tool traverse speed of 60 mm/min

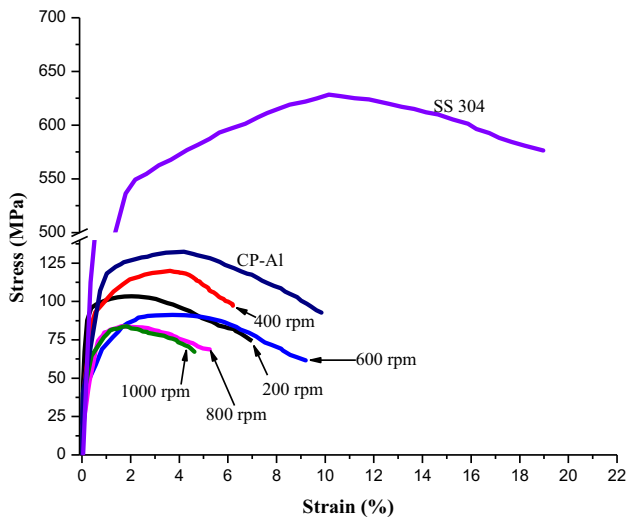


Fig. 9 Tensile properties of friction stir welded joints and base material at room temperature for varying tool rotational speeds

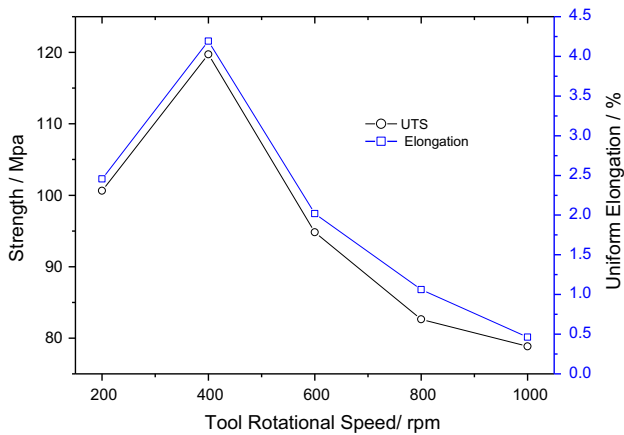


Fig. 10 Tensile strength and percentage elongation at varying tool rotational speeds

indentations were taken at an interval of 10 μm . The results are shown in Fig. 13. The hardness profiles were carried out at different zones, and interaction between successive indentations was minimized to the greatest possible extent. The microhardness variation of different welded joints by varying rotational speeds is shown in Fig. 14. The hardness reaches the peak at the interface of the welded sample. Mahto et al. (Ref 32) have reported of the maximum hardness value at the interface zone, indicating more brittle nature of the interface due to the stirring action of the pin leading to excessive plastic deformation and recrystallization. The grain size and brittle intermetallics influenced hardness values. The hardness decreased slightly in TMAZ of CP Al at the retreating side, which indicated second phase particle dissolution and coarsening caused by thermo-mechanical effect due to dynamic recovery and recrystallization (Ref 1). The decrease in hardness at the HAZ is due to the dissolution of the precipitates during welding. The increase in the hardness of the SS (near the interface) is directly related to high deformation. The maximum hardness value of the welded joint was observed for the joints processed at 1000 rpm.

4. Conclusions

1. The grain structure of CP Al side underwent severe plastic deformation accompanied by dynamic recrystallization. The grain structural change in stainless steel side was minimal due to the offset of tool toward the CP Al side. Fine particles of stainless steel were distributed over the CP Al side.
2. The intermetallic layer thickness increased with increase in rotational speed. The intermetallic phases like FeAl_2 , $\text{Al}_{13}\text{Fe}_4$ and Al_5Fe_2 were detected in x-ray diffraction patterns. The intermetallic compound formed at the weld nugget was FeAl_3 .
3. The tensile strength of the welded joints showed the maximum value of about $\sim 90\%$ of CP Al at 400 rpm tool rotational speed and the tensile strength decreased gradually with the increase in tool rotational speed due to an increase in the volume fraction of brittle inter-

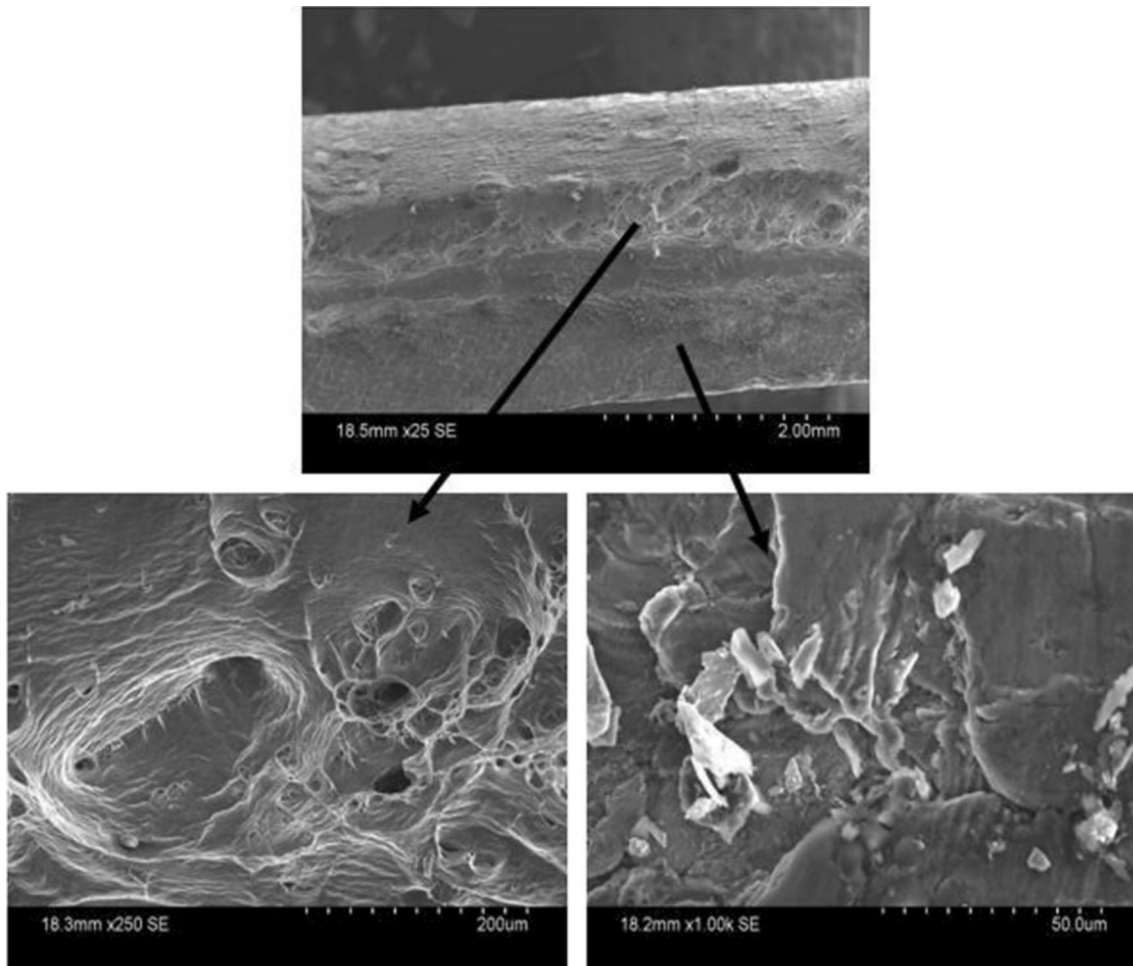


Fig. 11 Fractured surface of tensile sample on aluminum side

metallics. However, at a tool rotational speed of 200 rpm, heat generation and mixing of material were not enough to make a good joint.

4. Hardness value reached a maximum at the stir zone due to the formation of brittle intermetallics. With an increase

in rotational speed, hardness value of the stir zone increased due to an increase in temperature promoting the formation of more intermetallics.

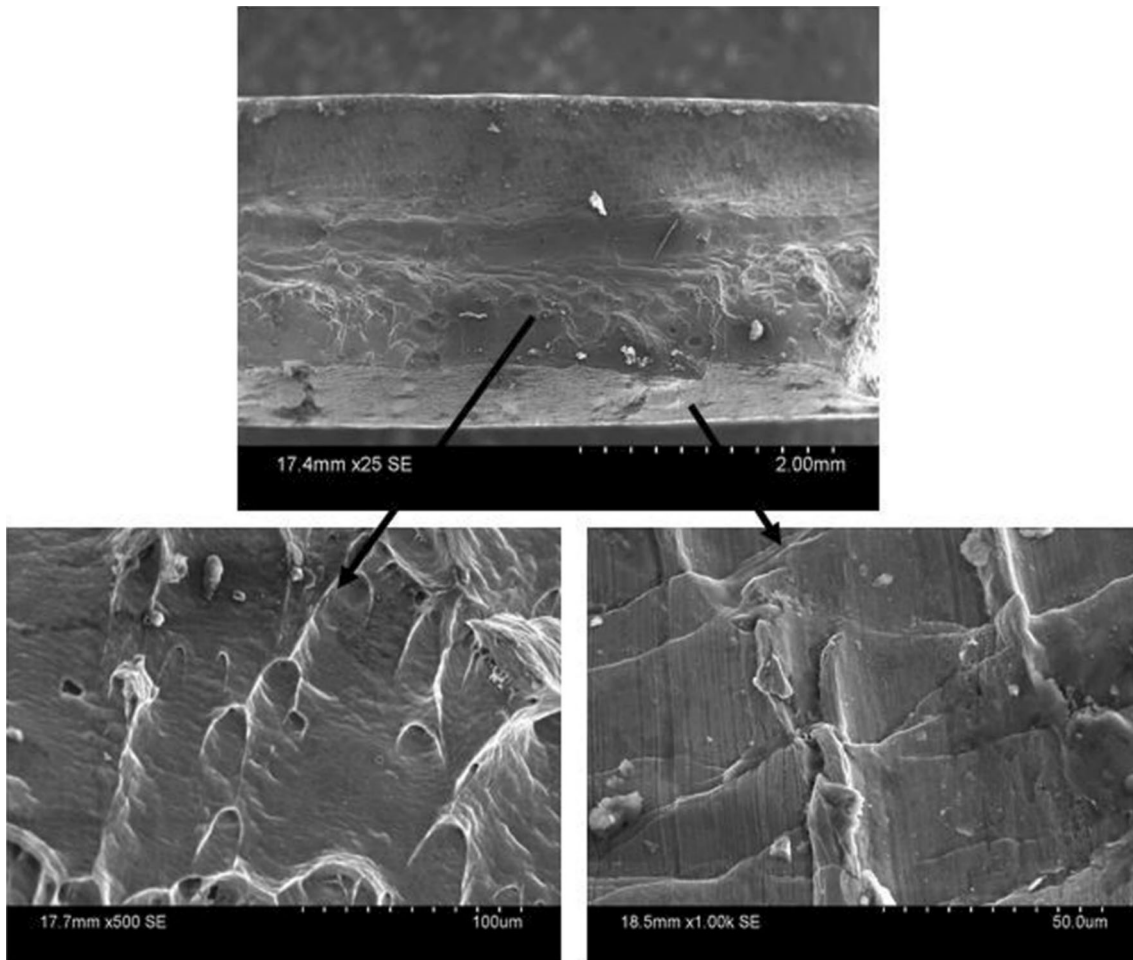


Fig. 12 Fractured surface of tensile sample on SS side

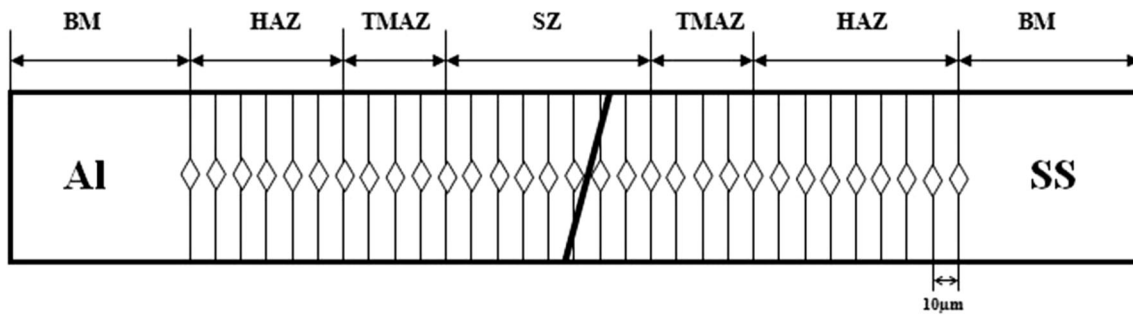


Fig. 13 Schematic sketch of the arrangement of microhardness indentation across the interfaces of friction stir welded sample

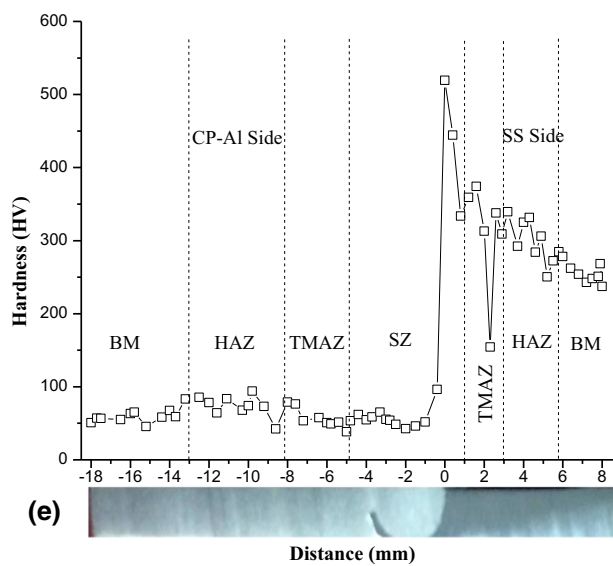
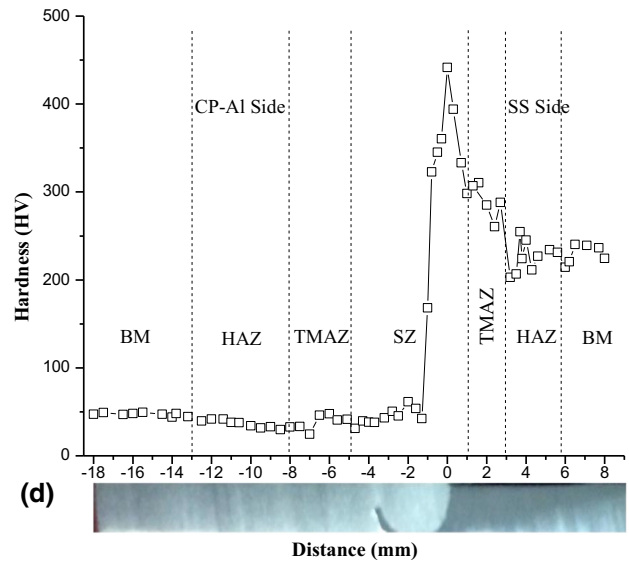
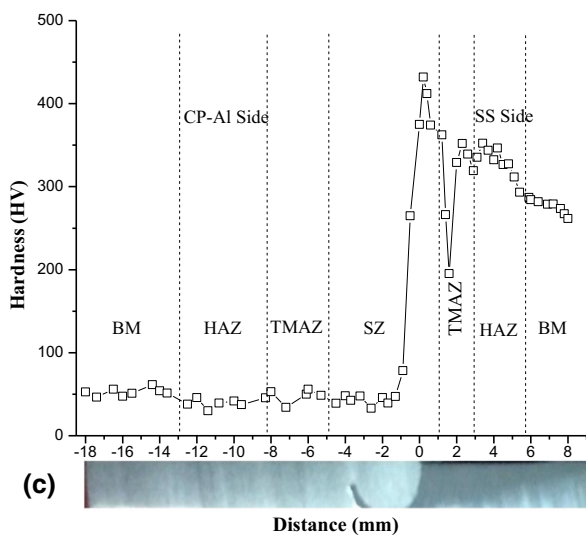
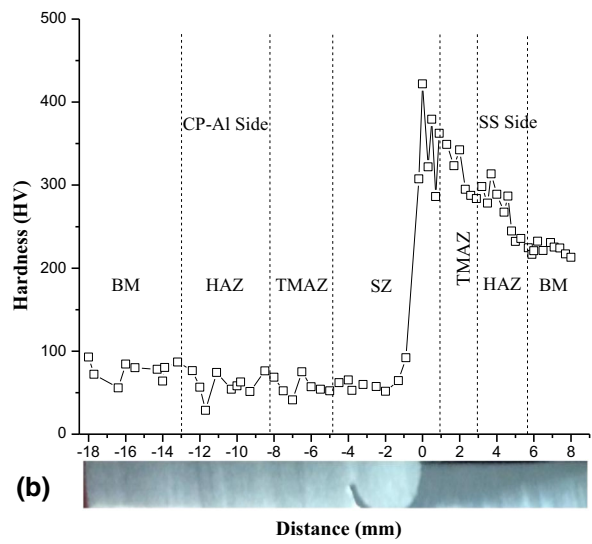
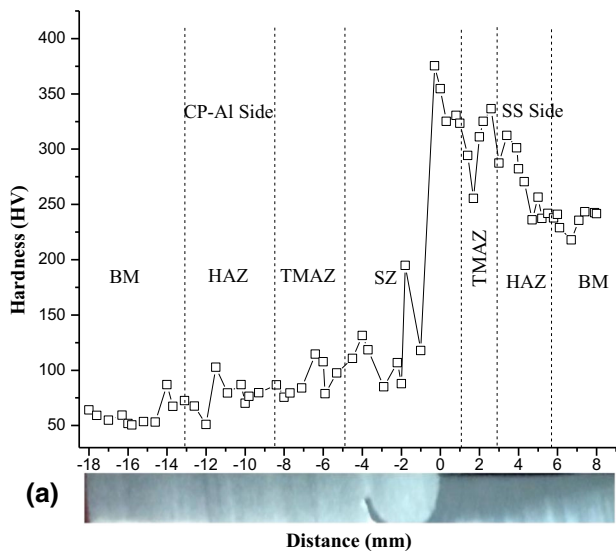


Fig. 14 Hardness profile of varying tool rotational speeds (a) 200 rpm, (b) 400 rpm, (c) 600 rpm, (d) 800 rpm and (e) 1000 rpm

References

1. R.S. Mishra, P.S. De, and N. Kumar, *Friction Stir Welding and Processing: Science and Engineering*, Springer, Berlin, 2014
2. M. Habibnia, M. Shakeri, S. Nourouzi, and M.K. Besharati Givi, Microstructural and Mechanical Properties of Friction Stir Welded 5050 Al Alloy and 304 Stainless Steel Plates, *Int. J. Adv. Manuf. Technol.*, 2015, **76**(5–8), p 819–829
3. M. Ghosh, R. Gupta, and M. Husain, Friction Stir Welding of Stainless Steel to Al Alloy: Effect of Thermal Condition on Weld Nugget Microstructure, *Metall. Mater. Trans. A*, 2014, **45**(2), p 854–863
4. X. Liu, S. Lan, and J. Ni, Analysis of Process Parameters Effects on Friction Stir Welding of Dissimilar Aluminium Alloy to Advanced High Strength Steel, *Mater. Des.*, 2014, **59**, p 50–62
5. V. Satyanarayana, G.M. Reddy, and T. Mohandas, Dissimilar Metal Friction Welding of Austenitic-Ferritic Stainless Steels, *J. Mater. Process. Technol.*, 2005, **160**(2), p 128–137
6. H. Uzun, C. Dalle Donne, A. Argagnotto, T. Ghidini, and C. Gambaro, Friction Stir Welding of Dissimilar Al 6013-T4 to X5CrNi18-10 Stainless Steel, *Mater. Des.*, 2005, **26**, p 41–46
7. S. Fukumoto, H. Tsubakino, K. Okita, M. Aritoshi, and T. Tomita, Amorphization by Friction Welding between 5052 Aluminium Alloy and 304 Stainless Steel, *Scr. Mater.*, 2000, **42**(8), p 807–812
8. U.K. Mudali, A. Ravishankar, S. Ningshen, G. Suresh, R. Sole, and K. Thyagarajan, Materials Development and Corrosion Issues in the Back End of Fuel Cycle, *Energy Procedia*, 2011, **7**, p 468–473
9. M. Ghosh, A. Kar, K. Kumar, and S.V. Kailas, Structural Characterisation of Reaction Zone for Friction Stir Welded Aluminium-Stainless Steel Joint, *Mater. Technol.*, 2012, **27**(2), p 169–172
10. V. Ryabov, *Welding of Aluminium Alloys to Steels*, Harwood Academic, London, 1998
11. T. Ogura, T. Nishida, Y. Tanaka, H. Nishida, S. Yoshikawa, M. Fujimoto, and A. Hirose, Microscale Evaluation of Mechanical Properties of Friction Stir Welded A6061 Aluminium Alloy/304 Stainless Steel Dissimilar Lap Joint, *Sci. Technol. Weld. Join.*, 2013, **18**(2), p 108–113
12. T. Sakthivel, G. Sengar, and J. Mukhopadhyay, Effect of Welding Speed on Microstructure and Mechanical Properties of Friction-Stir-Welded Aluminium, *Int. J. Adv. Manuf. Technol.*, 2009, **43**(5–6), p 468–473
13. H. Bang, H. Bang, G. Jeon, I. Oh, and C. Ro, Gas Tungsten Arc Welding Assisted Hybrid Friction Stir Welding of Dissimilar Materials Al6061-T6 Aluminium Alloy and STS304 Stainless Steel, *Mater. Des.*, 2012, **37**, p 48–55
14. T. Chen, Process Parameters Study on FSW Joint of Dissimilar Metals for Aluminium-Steel, *J. Mater. Sci.*, 2009, **44**(10), p 2573–2580
15. S. Fukumoto, H. Tsubakino, K. Okita, M. Aritoshi, and T. Tomita, Microstructure of Friction Weld Interface of 1050 Aluminium to Austenitic Stainless Steel, *Mater. Sci. Technol.*, 1998, **14**(4), p 333–338
16. A. Elrefaey, M. Gouda, M. Takahashi, and K. Ikeuchi, Characterization of Aluminum/Steel Lap Joint by Friction Stir Welding, *J. Mater. Eng. Perform.*, 2005, **14**(1), p 10–17
17. H. Das, S. Jana, T. Pal, and A. De, Numerical and Experimental Investigation on Friction Stir Lap Welding of Aluminium to Steel, *Sci. Technol. Weld. Join.*, 2014, **19**(1), p 69–75
18. T. Ogura, Y. Saito, T. Nishida, H. Nishida, T. Yoshida, N. Omichi, M. Fujimoto, and A. Hirose, Partitioning Evaluation of Mechanical Properties and the Interfacial Microstructure in a Friction Stir Welded Aluminium Alloy/Stainless Steel Lap Joint, *Scr. Mater.*, 2012, **66**(8), p 531–534
19. T. Ishikawa, H. Fujii, K. Genchi, S. Iwaki, S. Matsuoka, and K. Nogi, High Speed-High Quality Friction Stir Welding of Austenitic Stainless Steel, *ISIJ Int.*, 2009, **49**(6), p 897–901
20. A. Lakshminarayanan, V. Balasubramanian, and K. Elangovan, Effect of Welding Processes on Tensile Properties of AA6061 Aluminium Alloy Joints, *Int. J. Adv. Manuf. Technol.*, 2009, **40**(3–4), p 286–296
21. A. Hassan, A.F. Norman, D.A. Price, and P.B. Prangnell, Stability of Nugget Zone Grain Structures in High Strength Al-Alloy Friction Stir Welds during Solution Treatment, *Acta Mater.*, 2003, **51**, p 1923–1936
22. S. Kundu, D. Roy, R. Bhola, D. Bhattacharjee, B. Mishra, and S. Chatterjee, Microstructure and Tensile Strength of Friction Stir Welded Joints between Interstitial Free Steel and Commercially Pure Aluminium, *Mater. Des.*, 2013, **50**, p 370–375
23. W.J. Arbegast, Z. Jin, A. Beaudoin, T.A. Bieler, and B. Radhakrishnan, *Hot Deformation of Aluminum Alloys III*, TMS, Warrendale, PA, 2003, p 313–327
24. H. Baker, Ed., *ASM Handbook: Alloy Phase Diagrams*, Vol 3, ASM International, Materials Park, OH, 1992
25. W.B. Lee, M. Schmuecker, U.A. Mercardo, G. Biallas, and S.B. Jung, Interfacial Reaction in Steel-Aluminium Joints made by Friction Stir Welding, *Scr. Mater.*, 2006, **55**(4), p 355–358
26. Y. Wei, J. Li, J. Xiong, and F. Zhang, Effect of Tool Pin Insertion Depth on Friction Stir Lap Welding of Aluminium to Stainless Steel, *J. Mater. Eng. Perform.*, 2013, **22**(10), p 3005–3013
27. A. Yazdipour and A. Heidarzadeh, Dissimilar Butt Friction Stir Welding of Al 5083-H321 and 316L Stainless Steel Alloys, *Int. J. Adv. Manuf. Technol.*, 2016, **87**, p 3105–3112
28. M. Sahin, Characterization of Properties in Friction-Welded Austenitic-Stainless Steel and Aluminium Joints, *Ind. Lubr. Tribol.*, 2014, **66**(2), p 260–271
29. S. Bozzi, A. Helbert-Etter, T. Baudin, B. Criqui, and J.G. Kerbiguet, Intermetallic Compounds in Al 6016/IF-Steel Friction Stir Spot Welds, *Mater. Sci. Eng. A*, 2010, **527**, p 4505–4509
30. L. Agudo, D. Eyidi, C.H. Schmaranzer, E. Arenholz, N. Jank, J. Bruckner, and A.R. Pyzalla, Intermetallic Fe_xAl_y-Phases in a Steel/Al-Alloy Fusion Weld, *J. Mater. Sci.*, 2007, **42**(12), p 4205–4214
31. M. Yılmaz, M. Çöl, and M. Acet, Interface Properties of Aluminium/Steel Friction-Welded Components, *Mater. Charact.*, 2002, **49**(5), p 421–429
32. R.P. Mahto, R. Bhoje, S.K. Pal, H.S. Joshi, and S. Das, A Study on Mechanical Properties in Friction Stir Lap Welding of AA 6061-T6 and AISI, 304, *Mater. Sci. Eng. A*, 2016, **652**, p 136–144